IEEE Access
Multidisciplinary | Rapid Review | Open Access Journal

Received September 23, 2018, accepted October 22, 2018, date of publication November 9, 2018,
date of current version December 3, 2018.

Digital Object Identifier 10.1109/ACCESS.2018.2879326

Closed-Form Formulas of Input Impedance and Axial Ratio of a Circular Patch With Perturbation Segments

NU PHAM[1], JAE-YOUNG CHUNG[1], (Senior Member, IEEE), AND KYUNG-YOUNG JUNG[2], (Senior Member, IEEE)

[1]Department of Electrical and Information Engineering, Seoul National University of Science and Technology, Seoul 01811, South Korea
[2]Department of Electronic Engineering, Hanyang University, Seoul 04763, South Korea

Corresponding author: Kyung-Young Jung (kyjung3@hanyang.ac.kr)

This work was supported by the National Research Foundation of Korea (NRF) through the Basic Science Research Program funded by the Ministry of Education under Grant 2017R1D1A1B03034537.

ABSTRACT We present a simple and useful closed-form expression to compute antenna input impedance and the axial ratio of a circular patch antenna with perturbation segments. The closed-form expression is obtained by applying the cavity perturbation theory on antenna equivalent circuits that represent the resonant behaviors of two degenerated modes in the antenna. In particular, we exclude the assumption that equal resistance occurs between two modes and include the perturbation shape parameters in the proposed formulas, which results in a more accurate prediction of the antenna input impedance and axial ratio. The validity of the proposed equations is demonstrated by comparing the analytical results to full-wave simulations and measurements.

INDEX TERMS Antenna, axial ratio, cavity perturbation theory, circular patch antenna, circular polarization, input impedance.

I. INTRODUCTION

Closed-form formulas of antenna parameters are useful in understanding the physical insights of the antenna. They are also practical for defining antenna geometry with less computational effort relative to rigorous simulation techniques. Several studies have examined closed-form formulas for microstrip patch antennas with different shapes, feeding methods, and polarizations. Derneryd and Lind [1] first published the closed-form formulas of the input impedance of a linearly polarized rectangular patch antenna based on the resonant cavity model. Jackson and Alexopoulos [2] derived formulas of input resistance, bandwidth (BW), and radiation efficiency for a rectangular patch by combining Sommerfeld integrals of magnetic vector potential and cavity model analysis. Langston and Jackson [3] contributed pioneering studies on estimating impedance bandwidth, and axial ratio (AR) of circularly polarized (CP) rectangular patch antennas. These closed-form formulas are derived by means of a clever arrangement of the antenna's reactance in terms of its quality factor (Q-factor) and resonant frequency inside the patch cavity.

The goal of this study is to derive closed-form formulas for antenna input impedance and the axial ratio of a single-fed CP circular patch antenna with perturbation segments. This design method is known to be the simplest means of introducing CP by generating two degenerated modes that have equal amplitude but a 90° phase difference inside the microstrip patch cavity.

Several studies have been conducted to examine the CP mechanism of this type of antenna and to identify useful antenna design formulas. The studies in [4] and [5] analyzed the position of feed and the dimensions of a rectangular patch to achieve CP based on cavity analysis. In [6], the boundary element and perturbation method were used to verify the mode degeneracy in a circular patch according to locations of perturbation segments and feeding points. In [7], the CP of a perturbed circular patch was used to relate the ratio of perturbation segments and patch areas to the antenna quality factor. This is achieved by calculating eigenvalues of the two degenerated modes from a variable separation method and modeling the modes into resistor-inductor-capacitor (RLC) tanks.

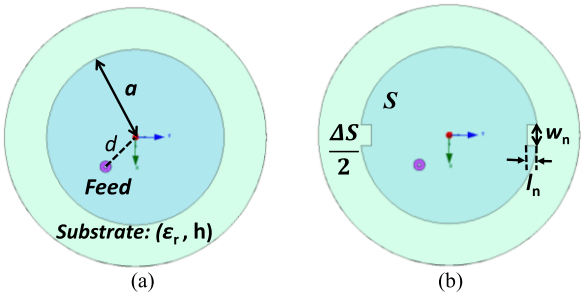

FIGURE 1. Top views of circular patch antenna (a) without and (b) with perturbation segments.

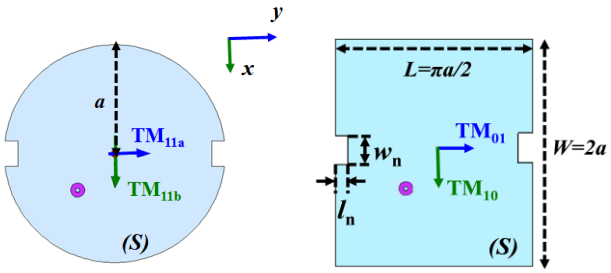

FIGURE 2. Equivalent transformation of a circular patch with segments to a rectangular patch with the same segments.

Our study takes a step forward from [7] by considering the segment's length and width when calculating the input impedance of a circular patch. Moreover, the proposed formula improves the accuracy in predicting input impedance, as it is not derived based on the assumption of equal resistance between the two degenerate modes. Subsequently, the AR formula of the antenna is obtained by applying the derived input impedance into the Poincare sphere representation. With this formula, the AR performance can be accurately predicted without the far-field radiation characteristics of the antenna. The formula is also useful to identify the optimal dimensions of perturbation segments necessary to achieve the best AR performance and to estimate the AR bandwidth of the antenna.

The derivation process of the proposed formulas is described in detail in the following sections. Specifically, Section II derives the resonant frequencies of the two degenerate modes in terms of the length and width of perturbation segments. With these resonant frequencies, the impedances of two degenerated modes can be computed separately from two equivalent cavity models. This process is described in Section III. In Section IV, we describe the derivation of the AR formula. Section V validates the results obtained from the proposed formulas by comparing them with the full-wave simulation data and antenna prototype measurement data.

II. RESONANT FREQUENCIES OF TWO DEGENERATE MODES

Fig. 1 depicts a single feed circular patch antenna, where (a) is without and (b) is with perturbation segments. These segments are all fed with an offset d from the center using a 50-ohm coaxial probe. The rectangular perturbation segment has an area of $\Delta S/2 = l_{\rm n} \cdot w_{\rm n}$. Two degenerate modes are induced by these segments and their resonant frequencies shift from the resonant frequency of the original $\rm TM_{11}$ mode without perturbations.

The cavity perturbation method can be used to determine the amount of frequency shift. In [7], the frequency shift was calculated from the eigenvalues of two degenerated modes using the variable separation method and expressed in the form of the area of perturbation segments (ΔS). Our interest is to extend this frequency shift in the form of a segment's length ($l_{\rm n}$) and width ($w_{\rm n}$).

Using the perturbation theory, we can determine the ratio between the amount of frequency shift ($\Delta\omega$) and the $p^{\rm th}$ mode resonant frequency ($\omega_{\rm p}$) from the ratio of stored energy in the segment with volume ΔV and patch cavity with volume V:

$$\frac{\Delta\omega}{\omega_p} = \frac{\int_{\Delta V}\left(\varepsilon\vec{E_p}\cdot\vec{E_p}^* - \mu\vec{H_p}\cdot\vec{H_p}^*\right)dV}{\int_V\left(\mu\vec{H_p}\cdot\vec{H_p}^* + \varepsilon\vec{E_p}\cdot\vec{E_p}^*\right)dV} = \frac{\int_{\Delta V}\left(\varepsilon\left|\vec{E_p}\right|^2 - \mu\left|\vec{H_p}\right|^2\right)dV}{2\int_V \varepsilon\left|\vec{E_p}\right|^2 dV} \quad (1)$$

where $E_{\rm p}$ and $H_{\rm p}$ are the electric and magnetic field of the $p^{\rm th}$ mode, and ε and μ are the permittivity and permeability of the substrate, respectively.

To facilitate analysis, the circular patch with rectangular segments is transformed to a rectangular patch having the same segments. This can be performed as long as the stored energy between the two patches is identical [8]. The equivalent geometry of the rectangular patch is $W = 2a$ and $L = \pi a/2$, as depicted in Fig. 2, where the size of the rectangular segments remains the same.

Once the transformation to a rectangular patch has occurred, the resonant frequency shift from the dominant $\rm TM_{11}$ mode to the two degenerated modes, $\rm TM_{11a}$ and $\rm TM_{11b}$, in the circular patch can be considered as equivalent to the frequency shift of $\rm TM_{10}$ and $\rm TM_{01}$ in the rectangular patch (see Fig. 2). This approximation is valid because the amounts of energy inside the cavity and perturbation area of the rectangular patch are equivalent to those of the circular patch. Applying this to (1) for the two degenerated modes gives:

$$\frac{\Delta\omega_{11a}}{\omega_{11}} \approx \frac{\Delta\omega_{01}}{\omega_{11}} = \frac{\int_{\Delta V}\left(\varepsilon\left|E_{01}\right|^2 - \mu\left|H_{01}\right|^2\right)dV}{2\int_V \varepsilon\left|E_{11}\right|^2 dV}, \quad (2)$$

$$\frac{\Delta\omega_{11b}}{\omega_{11}} \approx \frac{\Delta\omega_{10}}{\omega_{11}} = \frac{\int_{\Delta V}\left(\varepsilon\left|E_{10}\right|^2 - \mu\left|H_{10}\right|^2\right)dV}{2\int_V \varepsilon\left|E_{11}\right|^2 dV}. \quad (3)$$

Analytical solutions for the field quantities of each mode can be found in [9] and [10] and are outlined in Appendix A in this study. Substituting these field quantities in (2) and (3) yields:

$$\frac{\Delta\omega_{11a}}{\omega_{11}} = \left(\frac{A_{01}}{A_{11}}\right)^2 \frac{1}{0.375\pi}\frac{l_n}{a}\sin\left(\frac{\pi w_n}{2a}\right), \quad (4)$$

$$\frac{\Delta\omega_{11b}}{\omega_{11}} = \left(\frac{A_{10}}{A_{11}}\right)^2 \frac{\pi}{1.5}\frac{l_n}{a}\sin\left(\frac{2w_n}{a}\right), \quad (5)$$

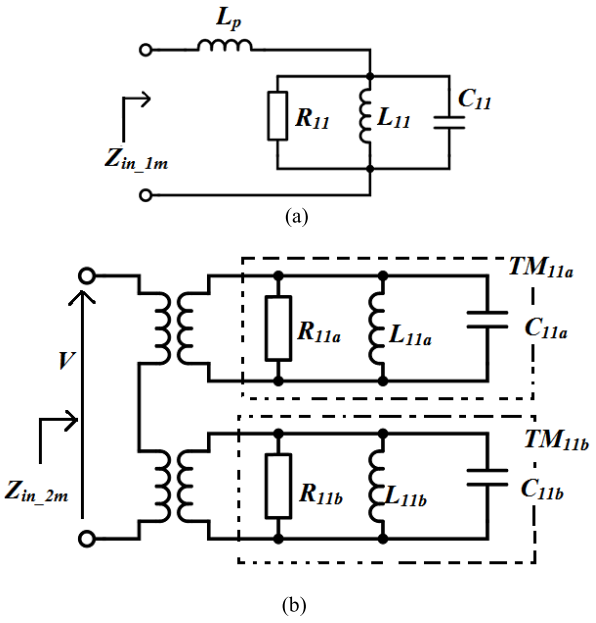

FIGURE 3. Equivalent circuit models of circular patch antennas with (a) a single TM_{11} mode and (b) two degenerated modes.

where A_{01}, A_{10}, and A_{11} are given in the Appendix A. It is observed in (4) and (5) that the resonant frequency shifts of each degenerated mode are in a function of not only the patch diameter but also the length and width of the perturbation segments.

III. INPUT IMPEDANCE AND AXIAL RATIO

A. INPUT IMPEDANCE

Using the resonant frequencies calculated in the previous section, the input impedance of the CP antenna with two degenerated modes is derived from the equivalent circuit analysis. Fig. 3(a) and (b) are equivalent circuits of the circular patches shown in Fig. 1(a) and (b), without and with perturbation segments, respectively. In Fig. 3(a), the input impedance is denoted as $Z_{\text{in\_1m}}$, which combines a parallel RLC tank resulting from the dominant TM_{11} mode and the inductive component L_p representing the probe inductance. In Fig. 3(b), the two degenerated modes are represented by two independent RLC tanks and the overall input impedance is denoted as $Z_{\text{in\_2m}}$.

Based on the equivalent circuit analysis [11], $Z_{\text{in\_1m}}$ in Fig. 3(a) is obtained by:

$$Z_{in\_1m} = jX_p + \frac{R_{11}}{1 + j2Q\left(\frac{\omega}{\omega_{11}} - 1\right)}, \tag{6}$$

where Q and R_{11} are the Q-factor and input resistance of the parallel cavity at ω_{11}, which is the resonance frequency of TM_{11} mode. X_{p} is the reactance of the probe inductance which induces an additional shift in the resonance frequency. Considering this, (6) can be re-written as:

$$Z_{in\_1m} = \frac{R_{11}}{1 + j2Q\left(\frac{\omega}{\omega_{p11}} - 1\right)} = \frac{R_{11}}{1 + jX}, \tag{7}$$

where $X = 2Q(\omega/\omega_{p11} - 1)$ and ω_{p11} is the resonance frequency shifted from ω_{11} as a result of the probe effect.

Similarly, $Z_{\text{in\_2m}}$ in Fig. 3(b) is obtained by:

$$\begin{aligned} Z_{in\_2m} &= \frac{R_{11a}}{1 + j2Q\left(\frac{\omega}{\omega_{p11a}} - 1\right)} + \frac{R_{11b}}{1 + j2Q\left(\frac{\omega}{\omega_{p11b}} - 1\right)} \\ &= \frac{R_{11a}}{1 + jA} + \frac{R_{11b}}{1 + jB}, \end{aligned} \tag{8}$$

where $R_{11\text{a}}$ and $R_{11\text{b}}$ are the input resistances of the two degenerated modes, $TM_{11\text{a}}$ and $TM_{11\text{b}}$, respectively; and $\omega_{p11\text{a}}$ and $\omega_{p11\text{b}}$ are the resonance frequencies of the two modes considering the frequency shift due to the probe effect. These frequencies are related to ω_{p11} in (7) as:

$$\omega_{p11a} = \omega_{p11}\,(1 + \Delta\omega_{11a})\,; \quad \omega_{p11b} = \omega_{p11}\,(1 - \Delta\omega_{11b}), \tag{9}$$

where $\Delta\omega_{11a}$ and $\Delta\omega_{11b}$ are frequency shifts resulting from the perturbation segments found in (4) and (5). By using (9) and X defined in (7), we can express A and B in (8) as:

$$A = \frac{X - 2Q\Delta\omega_{11a}}{1 + \Delta\omega_{11a}}; \quad B = \frac{X + 2Q\Delta\omega_{11b}}{1 - \Delta\omega_{11b}}. \tag{10}$$

Furthermore, R_{11a} and R_{11b} can be expressed in terms of R_{11} with a scaling factor obtained by using the cavity model analysis [12], a process outlined in the Appendix B, and the results are:

$$R_{11a} = \frac{J_1^2(d\,k_{11a})}{J_1^2(a\,k_{11a})}\frac{J_1^2(a\,k_{11})}{J_1^2(d\,k_{11})}\frac{(a^2k_{11}^2 - 1)(1 + \Delta\omega_{11a})}{a^2k_{11}^2(1 + \Delta\omega_{11a}^2) - 1}R_{11}, \tag{11}$$

$$R_{11b} = \frac{J_1^2(d\,k_{11b})}{J_1^2(a\,k_{11b})}\frac{J_1^2(a\,k_{11})}{J_1^2(d\,k_{11})}\frac{(a^2k_{11}^2 - 1)(1 - \Delta\omega_{11b})}{a^2k_{11}^2(1 - \Delta\omega_{11b}^2) - 1}R_{11}, \tag{12}$$

where the wavenumbers of each degenerated mode are:

$$k_{11a} = \omega_{11a}\sqrt{\varepsilon\mu}; \quad k_{11b} = \omega_{11b}\sqrt{\varepsilon\mu}. \tag{13}$$

Consequently, $Z_{\text{in\_2m}}$ is calculated by plugging (10), (11), and (12) into (8).

B. AXIAL RATIO AND BANDWIDTH

Computing the axial ratio from the Poincare sphere representation is given in [13] as:

$$AR = \pm\cot(\varepsilon) = \pm\frac{1 + \sqrt{1 - \sin^2(2\varepsilon)}}{\sin(2\varepsilon)}. \tag{14}$$

The term $\sin(2\varepsilon)$ can be expressed with other angles using trigonometric relations in spherical coordinates as:

$$\sin(2\varepsilon) = \sin(2\gamma)\sin(\delta), \tag{15}$$

where γ and δ represent the amplitude ratio and phase difference, respectively, between the E-fields of the two degenerated modes. They are related to the parameters A, B, R_{11a}, and R_{11b} obtained previously:

$$\delta = \arg(Z_b) - \arg(Z_a) = \tan^{-1} A - \tan^{-1} B \quad (16)$$

$$\tan(\gamma) = \left|\frac{E_b}{E_a}\right| = \left|\frac{Z_b}{Z_a}\right| = \frac{R_{11b}}{R_{11a}}\sqrt{\frac{1+A^2}{1+B^2}} \quad (17)$$

where Z_a and Z_b are the impedances of the two degenerated modes, respectively. By using trigonometric identities, we obtain:

$$\sin(\delta) = \sin\left(\tan^{-1} A\right)\cos\left(\tan^{-1} B\right) - \cos\left(\tan^{-1} A\right)\sin\left(\tan^{-1} B\right) \quad (18)$$

$$\sin(2\gamma) = \frac{2\tan(\gamma)}{1+\tan^2(\gamma)}. \quad (19)$$

Substituting (18) and (19) into (15) yields:

$$\sin(2\varepsilon) = \frac{(A-B)\,R_{11a}R_{11b}}{\left(1+B^2\right)R_{11a}^2 + \left(1+A^2\right)R_{11b}^2} \quad (20)$$

Consequently, (20) is used in (14) to obtain the AR. We note that (20) is applicable to any antenna that supports two degenerated modes as long as the wavenumbers of each mode are known. We must only consider the amount of frequency shift resulting from perturbation, $\Delta\omega_{11a}$ and $\Delta\omega_{11b}$.

Having found the closed-form formula of the input impedance and AR, we can obtain the following useful equations that indicate the impedance matching bandwidth and AR bandwidth from [3]:

$$BW = \frac{1.1}{Q} \quad \text{and} \quad ARBW = \frac{0.27}{Q}, \quad (21)$$

where BW and $ARBW$ represent the matching bandwidth of voltage-standing-wave-ratio of less than 2 (VSWR $\leq$ 2) and AR bandwidth of less than 3 dB (AR $\leq$ 3 dB), respectively.

In addition, substituting (20) for (14) and letting the equation satisfy the condition of AR $\leq$ 3 dB, we can find the dimensions of perturbed segments to achieve such AR performance as:

$$l_n \sin\left(\frac{\pi w_n}{2a}\right) = \frac{0.315a}{Q+1} \quad (22)$$

IV. VALIDATION OF PROPOSED FORMULAS

In this section, the accuracy of the proposed formulas is evaluated by comparing the calculated input impedance and AR with full-wave simulation data and antenna prototype measurement data.

An antenna having the same geometry as in Fig. 1(b) is used. More specifically, the antenna is designed to resonate at 1.6 GHz with a patch radius of $a = 25.5$ mm and a probe feeding location of $d = 10$ mm from the center of the patch. The dimensions of the perturbation segments are $w_n = 11$ mm and $l_n = 2$ mm.

Fig. 4(a) and (b) shows a comparison of resistance and reactance of the antenna input impedance obtained from (8) and full-wave simulations. Also shown is the result using formulas in [3], which assumes the two degenerated modes have equal resistance values, namely $R_{11a} = R_{11b} = R_{11}$. As the figures indicate, the resistance and reactance calculated from the proposed formula show good agreement to the full-wave simulation results. In particular, the asymmetry in the resistances of the two degenerated modes can be

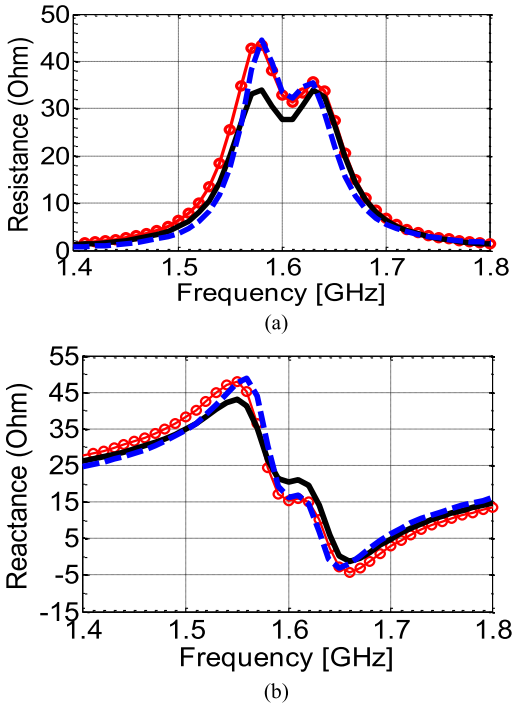

FIGURE 4. Comparison of the antenna input impedance calculated from the proposed formulas to the full-wave simulation data: (a) Resistance and (b) reactance.

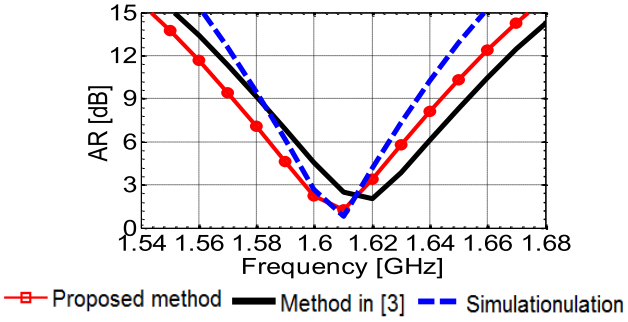

FIGURE 5. Comparison of the axial ratio calculated from the proposed formulas to the full-wave simulation data.

FIGURE 6. Pictures of fabricated antennas.

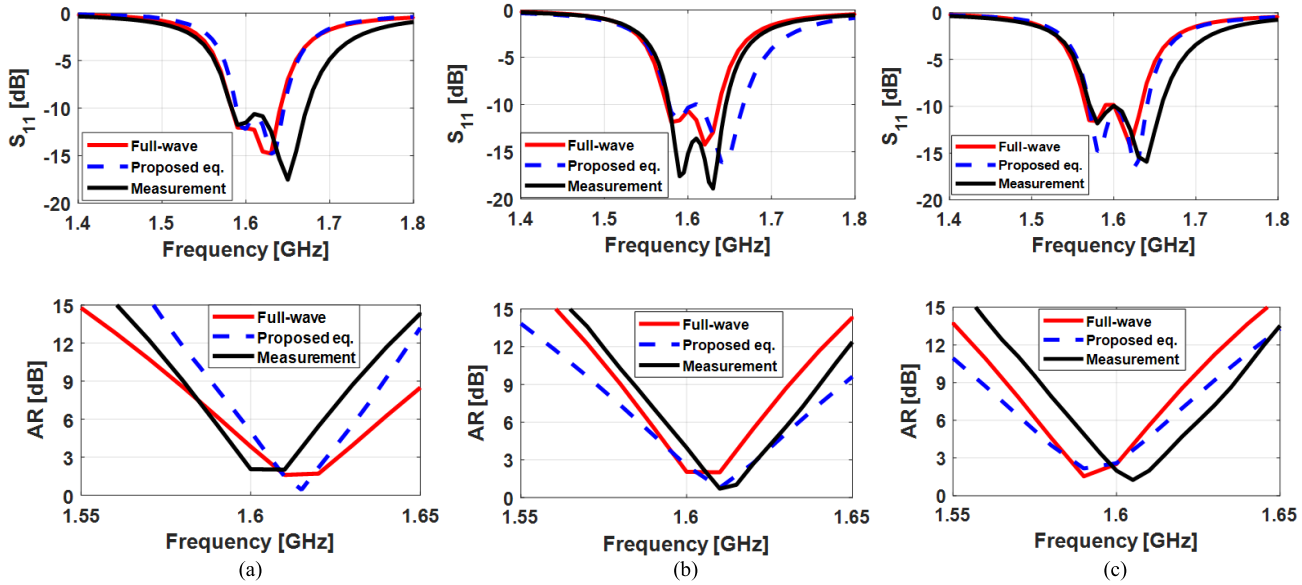

FIGURE 7. S_{11} and AR of three antennas with different perturbation segments obtained from full-wave simulations, proposed equations and prototype measurements: (a) Antenna 1, (b) Antenna 2 and (c) Antenna 3 followed by the label in Fig. 6.

TABLE 1. Comparison results with different value of Δ.

Parameters (mm)	Ant. 1	Ant. 2	Ant. 3
l_n	9.3	6	4.65
w_n	2	3.1	4

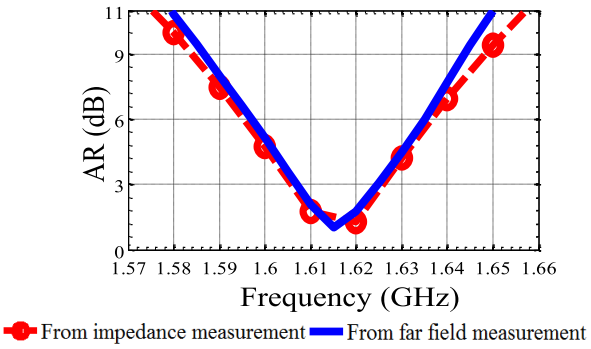

FIGURE 8. Comparison of AR calculated from the measured impedance and measured far-field data.

clearly captured. This aspect is not displayed in the result from [3]. Fig. 5 compares AR calculated from (14) to the full-wave simulation data. The minimal AR frequency and 3-dB ARBW show good agreement between the proposed formula and simulation, whereas the result from [3] shifts approximately 10 MHz.

Antennas having three different shapes of perturbation segments were next modeled and fabricated. This was necessary to evaluate whether the proposed formulas can accurately predict the input impedance and AR as w_n and l_n are altered. Table 1 shows the w_n and l_n values being investigated. As shown in Table 1, the area is fixed to $\Delta S/2 = 18.6$ mm^2. That the results are not changed when the formula in [7] is used since it only considers the segment's area not the shape. Fig. 6 show pictures of the three fabricated antennas.

Fig. 7 shows the S_{11} and AR for the three antennas obtained from (a) proposed formulas, (b) full-wave simulations, and (c) prototype measurements. The results from the proposed formulas show good agreement with the full-wave simulations. The results from the measurements show a slight discrepancy, which may be because of fabrication errors. However, they showed good agreement overall. We observed that both the resonant frequency and AR minimum frequency move to the lower frequency as the depth (l_n) of the perturbation segment lengthens (i.e., Ant. 1 to 3). This aspect cannot be observed if the previous formulas are used. Therefore, the proposed formulas are effective in predicting the input impedance and AR. In particular, the CP performance can be quickly estimated without time-consuming far-field measurements or extensive full-wave simulations.

V. CONCLUSION

Closed-form formulas of antenna input impedance and AR were presented for a circular patch antenna with perturbation segments. We first derived equations for the resonant frequencies of two degenerated modes based on the cavity perturbation theory together with an approximation of circular to rectangular patch cavity modes.

With these equations, the antenna input impedance and AR could be calculated by means of equivalent circuit analysis and Poincare sphere representation of polarization. These new formulas were in the form of length and width of perturbation segments (instead of the area as used in previous studies) Therefore, the impact of a segment's shape on antenna parameters could be investigated. In addition, the effect of

asymmetry between the two degenerated modes could be identified, which thus provides more accurate predictions in the input impedance and AR. The validity of the proposed equations was demonstrated by comparing the results to the full-wave simulation and measurement data.

We note that the proposed derivation steps and resulting formulas for the antenna input impedance were deemed valid for other types of CP antennas such as indented rectangular patch [15], [16], proximately coupled patch [17], or aperture coupled patch [18], as long as the eigenvalues of degenerated modes are known. Furthermore, the formula for calculating AR was found to be extremely useful. One can estimate AR with antenna impedance measured with a vector network analyzer without conducting far-field pattern measurements. For this purpose, parameters A and B that form the Poincare angles in (20) can be nicely rearranged in terms of the input impedance $Z_{\text{in\_2m}} = R_{\text{in}} + jX_{\text{in}}$ as:

$$B^2 = \frac{(R_{in} - R_{11a} - R_{11b})(R_{11b} - R_{in}) - X_{in}^2}{R_{in}^2 + X_{in}^2 - R_{in}R_{11a}}, \quad (23)$$

$$A = \frac{(R_{in} - R_{11a} - R_{11b}) - X_{in}B}{R_{in}B + X_{in}}. \quad (24)$$

Fig. 8 compares AR calculated from the measured impedance using the aforementioned equations and AR from the measured far-field patterns. The antenna used here was a circular patch whose segment's width and length were $w_{\text{n}} = 11$ mm, $l_{\text{n}} = 2$ mm. They show good agreement, especially at the useful AR < 3 dB frequency range.

APPENDIX

A. FIELD QUANTITIES IN CIRCULAR CAVITIY

Analytical solutions of electric fields inside circular and rectangular cavities for diagonally fed circular and rectangular patch antennas are expressed in [9] and [10] as:

$$E^{rect} = j\omega\mu \sum_m \sum_n A_{mn}^{rect} \cos\left(\frac{m\pi x}{W}\right) \cos\left(\frac{n\pi y}{L}\right), \quad (A.1)$$

$$E^{circ} = j\omega\mu \sum_m \sum_n A_{nm}^{circ} J_n\left(k_{nm}\rho\right) \cos n\left(\varphi - \pi\right), \quad (A.2)$$

where (A.1) and (A.2) are expressed in the rectangular (x, y) and cylindrical (ρ, ϕ) and coordinate conventions, respectively; J_{n} is the Bessel function, and k_{nm} is the wave number of the nm-th mode. The eigenvalues in (A.1) and (A.2) can be obtained by:

$$A_{mn}^{rect} = \frac{\varepsilon_m \varepsilon_n}{LW} \cos\left(\frac{m\,\pi\,x_{\text{f}}}{W}\right) \cos\left(\frac{n\,\pi\,y_{\text{f}}}{L}\right) \frac{1}{k^2 - k_{mn}^2} j_0 \times \left(\frac{m\,\pi\,\Delta}{2L}\right) j_0\left(\frac{n\pi\,\Delta}{2W}\right) \quad (A.3)$$

$$A_{nm}^{circ} = \frac{2\varepsilon_n J_n\left(k_{nm}d\right)\cos\left(n\pi\right)\sin n\Delta}{n\pi J_n^2\left(k_{nm}a\right)\left(a^2 - \frac{n^2}{k_{nm}^2}\right)\left(k^2 - k_{nm}^2\right)}, \quad (A.4)$$

where $\varepsilon_n = 1$ or 2 for $n = 0$ or $n \neq 0$, respectively, and (x_f, y_{f}) is the location of the feeding point. Δ is the width of the current source, empirically determined to be five times greater than the diameter of the coaxial probe to close the difference between measured and theoretical impedances. The wave number k_{nm} is:

$$k_{nm} = \sqrt{\left(\frac{m\pi}{W}\right)^2 + \left(\frac{n\pi}{L}\right)^2} \quad \text{and} \quad k_{nm} = \frac{\chi_{nm}}{a} \quad (A.5)$$

for the rectangular and circular patch cavity, respectively.

E_{10} and E_{01} of rectangular patch is obtained from (A.1) and (A.3) as:

$$\begin{cases} E_{01} = A_{01}\cos\left(\dfrac{\pi y}{L}\right) \\ H_{01} = -\dfrac{j}{\omega\mu}\dfrac{\partial E_{01}}{\partial y} = \dfrac{j}{\omega\mu}A_{01}\dfrac{\pi}{L}\sin\left(\dfrac{\pi y}{L}\right) \end{cases} \quad (A.6)$$

$$\begin{cases} E_{10} = A_{10}\cos\left(\dfrac{\pi x}{W}\right) \\ H_{10} = -\dfrac{j}{\omega\mu}\dfrac{\partial E_{10}}{\partial x} = \dfrac{j}{\omega\mu}A_{10}\dfrac{\pi}{W}\sin\left(\dfrac{\pi x}{W}\right), \end{cases} \quad (A.7)$$

and E_{11} obtained from (A.2) and (A.4) as:

$$E_{11} = A_{11}J_1(k_{11}\rho)\cos\varphi \quad (A.8)$$

With these field equations, the components in the numerator and denominator of (2) and (3) are found as:

$$\begin{aligned} &\varepsilon \iiint_{\Delta V} |E_{01}|^2 dV \\ &= \varepsilon\, h A_{01}^2 \int_{-w_n/2}^{w_n/2} dx \int_{L-l_n}^{L} \cos^2\left(\frac{\pi y}{L}\right) dy \\ &= \varepsilon\, h A_{01}^2\, l_n \int_{-w_n/2}^{w_n/2} \cos^2\left(\frac{\pi y}{L}\right) dy, \end{aligned} \quad (A.9)$$

$$\begin{aligned} &\mu \iiint_{\Delta V} |H_{01}|^2 dV \\ &= \mu\, h \frac{A_{01}^2}{\omega^2\mu^2}\frac{\pi^2}{L^2} \int_{-w_n/2}^{w_n/2} dx \int_{L-l_n}^{L} \sin^2\left(\frac{\pi y}{L}\right) dy \\ &= \varepsilon\, h A_{01}^2\, l_n \int_{-w_n/2}^{w_n/2} \sin^2\left(\frac{\pi y}{L}\right) dy, \end{aligned} \quad (A.10)$$

$$\begin{aligned} &\varepsilon \iiint_{\Delta V} |E_{11}|^2 dV \\ &= \varepsilon\, h A_{11}^2 \int_0^{2\pi} \int_0^a J_1^2\left(k_{11}\rho\right)\cos^2(\phi)\rho\, d\rho\, d\phi \\ &= \frac{\varepsilon\, h\pi\, a^2}{4} J_1^2(k_{11}a)\left(1 - \frac{1}{(k_{11}a)^2}\right). \end{aligned} \quad (A.11)$$

B. CLOSED-FORM EXPRESSIONS OF R_{11}, R_{11a}, R_{11b}

The cavity model analysis shows the results of input impedance Z_{nm} of the circular patch antenna for the nm-th modes with m, n $\neq 0$ in [12] as:

$$Z_{in} = j\,\omega\,\mu \sum_{n=1}^{\infty}\sum_{m=1}^{\infty}\left(\frac{\sin n\Delta}{n\Delta}\right)^2 \frac{J_n^2\left(k_{nm}d\right)}{J_n^2\left(k_{nm}a\right)} \times \frac{2\,h\,k_{nm}^2}{\pi\,\left\{k_{nm}^2 - k^2\left(1 - j\,\delta_{eff}\right)\right\}\left(k_{nm}^2\,a^2 - n^2\right)}, \quad (B.1)$$

where d is the distance of the feeding point to the center of the circular patch. This equation can be abbreviated as:

$$Z_{in} = j\omega \sum_{n,m=1}^{\infty} \frac{\alpha_{nm}}{k_{nm}^2 - k^2\left(1 - j\delta_{eff}\right)}, \tag{B.2}$$

where the variable α_{nm}:

$$\alpha_{nm} = \left(\frac{\sin n\Delta}{n\Delta}\right)^2 \frac{2\,h\mu}{\pi} \frac{J_n^2\left(k_{nm}\,\rho_0\right)}{J_n^2\left(k_{nm}\,a\right)} \frac{k_{nm}^2\,\cos^2 n\,\phi_0}{\left(k_{nm}^2\,a^2 - n^2\right)}. \tag{B.3}$$

Modeling each mode in the patch cavity to an RLC parallel circuit tank, we can write the input impedance of the antenna in [14] as:

$$Z_{in} = \sum_{n,m=1}^{\infty} \frac{1}{G_{nm} + j\left[\omega C_{nm} - \frac{1}{\omega L_{nm}}\right]}. \tag{B.4}$$

From equations (B.4) and (B.2), the resonant input resistance of each nm-th in relation to the resonant resistance of antenna is found as:

$$R_{nm} = \frac{1}{G_{nm}} = \frac{\alpha_{nm}}{\omega_{nm}\delta_{eff}} = \frac{\alpha_{nm}\,Q}{\omega_{nm}}, \tag{B.5}$$

where δ_{eff} is the effective loss tangent of the substrate material, which is the inverse of Q-factor. δ_{eff} can be directly calculated from the substrate's loss tangent value and its form factor. Considering the TM_{11} mode as the dominant mode inside circular patch cavity, we can determine the resonant resistance of antenna as:

$$R_{11} = \frac{1}{G_{11}} = \frac{\alpha_{11}}{\omega_{11}\delta_{eff}} = \frac{\alpha_{11}Q}{\omega_{11}}. \tag{B.6}$$

Furthermore, the impedance values including perturbations (R_{11a} and R_{11b}) can be expressed by:

$$R_{11a} = \frac{1}{G_{11a}} = \frac{\alpha_{11a}}{\omega_{11a}\delta_{eff}} = \frac{\alpha_{11a}Q}{\omega_{11a}}, \tag{B.7}$$

$$R_{11b} = \frac{1}{G_{11b}} = \frac{\alpha_{11b}}{\omega_{11b}\delta_{eff}} = \frac{\alpha_{11b}Q}{\omega_{11b}}. \tag{B.8}$$

To find the relation between $R_{11\mathrm{a}}$, $R_{11\mathrm{b}}$ and R_{11}, we exploit the ratio between degenerated mode and original mode presented in (10) and (B.6) with (8):

$$\frac{R_{11a}}{R_{11}} = \frac{\alpha_{11a}\,Q\,\omega_{11}}{\omega_{11a}\,\alpha_{11}\,Q} = \frac{\alpha_{11a}\,\omega_{11}}{\omega_{11a}\,\alpha_{11}}, \tag{B.9}$$

$$\frac{R_{11b}}{R_{11}} = \frac{\alpha_{11b}Q\omega_{11}}{\omega_{11b}\alpha_{11}Q} = \frac{\alpha_{11b}\omega_{11}}{\omega_{11b}\alpha_{11}}. \tag{B.10}$$

In here, the difference between two degenerated modes and original mode depends on variables α in (B.3) and frequency difference which are found in (4) and (5) by using cavity theory. Variable α contains all antenna parameters from the substrate characteristics to the antenna dimensions.

REFERENCES

[1] A. Derneryd and A. Lind, "Extended analysis of rectangular microstrip resonator antennas," *IEEE Trans. Antennas Propag.*, vol. AP-27, no. 6, pp. 846–849, Nov. 1979.

[2] D. R. Jackson and N. G. Alexopoulos, "Simple approximate formulas for input resistance, bandwidth, and efficiency of a resonant rectangular patch," *IEEE Trans. Antennas Propag.*, vol. 39, no. 3, pp. 407–410, Mar. 1991.

[3] W. L. Langston and D. R. Jackson, "Impedance, axial-ratio, and receive-power bandwidths of microstrip antennas," *IEEE Trans. Antennas Propaga.*, vol. 52, no. 10, pp. 2769–2774, Oct. 2004.

[4] Y. T. Lo and W. F. Richards, "Perturbation approach to design of circularly polarised microstrip antennas," *Electron. Lett.*, vol. 17, no. 11, pp. 383–385, May 1981.

[5] S. K. Lee, A. Sambell, E. Korolkiewicz, and S. F. Ooi, "Analysis and design of a circular-polarized nearly-square-patch antenna using a cavity model," *Microw. Opt. Technol. Lett.*, vol. 46, no. 4, pp. 406–410, 2005.

[6] H. Ohmine and Y. Sunahara, "An analysis of single-feed circularly polarized microstrip antenna using boundary element method," *Electron. Commun. Jpn. Commun.*, vol. 79, no. 2, pp. 22–34, 1996.

[7] M. Haneishi, T. Nambara, and S. Yoshida, "Study on ellipticity properties of single-feed-type circularly polarised microstrip antennas," *Electron. Lett.*, vol. 18, no. 5, pp. 191–193, Mar. 1982.

[8] A. K. Verma and Nasimuddin, "Analysis of circular microstrip patch antenna as an equivalent rectangular microstrip patch antenna on iso/anisotropic thick substrate," *IEE Proc.-Microw., Antennas Propag.*, vol. 150, no. 4, pp. 223–229, Aug. 2003.

[9] K. F. Lee, K. M. Luk, and H. W. Lai, "Characteristics of the circular patch antenna," in *Microstrip Patch Antennas*. Singapore: World Scientific, 2011, ch. 5, pp. 97–98.

[10] W. Richards and Y. Lo, "Design and theory of circularly polarized microstrip antennas," in *Proc. IEEE Antennas Propag. Soc. Int. Symp.*, vol. 17, Jun. 1979, pp. 117–120.

[11] J. L. Volakis, *Antenna Engineering Handbook*. New York, NY, USA: McGraw-Hill, 2007, ch. 7, pp. 16–17.

[12] R. Garg, "Circular disk and ring antenna," in *Microstrip Antenna Design Handbook*. Norwood, MA, USA: Artech House, 2000, ch. 5, pp. 328–329.

[13] J. D. Kraus, "Basic antenna concepts," in *Antennas*. New York, NY, USA: McGraw-Hill, 1998, ch. 2, pp. 76–78.

[14] D. G. Fang, "Microstrip patch antennas," in *Antenna Theory and Microstrip Antennas*. Boca Raton, FL, USA: CRC Press, ch. 3, 2009, pp. 93–94.

[15] G. Byun, J.-C. Hyun, S. M. Seo, and H. Choo, "Optimum array configuration to improve null steering time for mobile CRPA systems," *J. Electromagn. Eng. Sci.*, vol. 16, no. 2, pp. 74–79, Apr. 2016.

[16] J. Hur, G. Byun, and H. Choo, "Design of small CRPA arrays with circular microstrip loops for electromagnetically coupled feed," *J. Electromagn. Eng. Sci.*, vol. 18, no. 2, pp. 129–135, Apr. 2018.

[17] N. Pham, J. Y. Chung, and B. Lee, "A proximity-fed antenna for dual-band GPS receiver," *Progr. Electromagn. Res.*, vol. 61, pp. 1–8, 2016.

[18] J.-H. Kim and B.-G. Kim, "Effect of feed substrate thickness on the bandwidth and radiation characteristics of an aperture-coupled microstrip antenna with a high permittivity feed substrate," *J. Electromagn. Eng. Sci.*, vol. 18, no. 2, pp. 101–107, Apr. 2018.

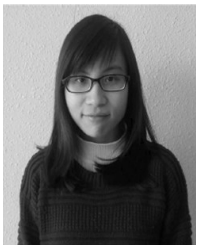

NU PHAM received the B.S. degree in telecommunication engineering from the Hanoi University of Science and Technology, Vietnam, in 2014, and the M.S. degree in electrical and information engineering from SeoulTech, South Korea, in 2016. She is currently an Engineer with Robert Bosch, Ho Chi Minh City, Vietnam. Her research interests are antenna theory and design.

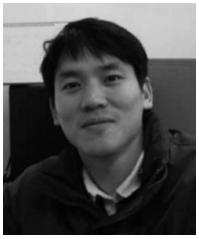

JAE-YOUNG CHUNG (SM'13) received the B.S. degree in electrical engineering from Yonsei University, South Korea, in 2002, and the M.S. and Ph.D. degrees in electrical engineering from The Ohio State University, USA, in 2007 and 2010, respectively. From 2002 to 2004, he was an RF Engineer with Motorola Korea. From 2010 to 2012, he was an Antenna Engineer with Samsung Electronics, South Korea. He is currently an Associate Professor with the Department of Electrical and Information Engineering, Seoul National University of Science and Technology (SeoulTech), South Korea. His research interests include electromagnetic measurement and antenna design.

KYUNG-YOUNG JUNG (SM'13) received the B.S. and M.S. degrees in electrical engineering from Hanyang University, Seoul, South Korea, in 1996 and 1998, respectively, and the Ph.D. degree in electrical and computer engineering from The Ohio State University, Columbus, USA, in 2008. From 2008 to 2009, he was a Post-Doctoral Researcher with The Ohio State University. From 2009 to 2010, he was an Assistant Professor with the Department of Electrical and Computer Engineering, Ajou University, Suwon, South Korea. Since 2011, he has been with Hanyang University, where he is currently an Associate Professor with the Department of Electronic Engineering. His current research interests include computational electromagnetics, bio electromagnetics, and nano electromagnetics. He received the Graduate Study Abroad Scholarship from the National Research Foundation of Korea, the Presidential Fellowship from The Ohio State University, the Best Teacher Award from Hanyang University, and the Outstanding Research Award from the Korean Institute of Electromagnetic Engineering Society.